Journal Name

ARTICLE TYPE

Cite this: DOI: 10.1039/xxxxxxxxxx

Elucidating the Mechanisms of Nanodiamond-Promoted Structural Disruption of Crystallised Lipid†

Zak E. Hughes,*[a] and Tiffany R. Walsh*[a]

Received Date
Accepted Date

DOI: 10.1039/xxxxxxxxxx

www.rsc.org/journalname

The removal or structural disruption of crystallised lipid is a pivotal but energy-intensive step in a wide range of industrial and biological processes. Strategies to disrupt the structure of crystallised lipid in aqueous solution at lower temperatures are much needed, where nanoparticle-based strategies show enormous promise. Using the aqueous tristearin bilayer as a model for crystallised lipid, we demonstrate that the synergistic use of surfactant and detonation nanodiamonds can depress the onset temperature at which disruption of the crystallised lipid structure occurs. Our simulations reveal the molecular-scale mechanisms by which this disruption takes place, indicating that the nanodiamonds serve a dual purpose. First, the nanodiamonds are predicted to facilitate delivery of surfactant to the lipid/water interface, and second, nanodiamond adsorption acts to roughen the lipid/water interface, enhancing ingress of surfactant into the bilayer. We find the balance of the hydrophobic surface area of the nanodiamond and the nanodiamond surface charge density to be a key determinant of the effectiveness of using nanodiamonds to facilitate lipid disruption. For the nanodiamond size considered here, we identify a moderate surface charge density, that ensures the nanodiamonds are neither too hydrophobic nor too hydrophilic, to be optimal.

The removal or breakdown of crystallised lipid is a key stage of many energy-intensive industrial processes. For example, the laundering of textiles is one of the most commonly and frequently practiced tasks in industrial settings world-wide, and therefore contributes substantially to global energy consumption.[1] In particular, laundering at hot temperatures (60°C or more) is required to remove the most challenging soil, sebum, typically conceptualised as crystallised lipid, even using modern detergents.[2–5] The high energy cost of removal under aqueous conditions is due to the fact that the triacylglycerol (TAG), or triglyceride, molecules which make up fats and oils typically require high temperatures even in the presence of surfactants. The enzymes that are present in many modern detergents are unable to hydrolyse crystallised lipid at room temperatures. Another example is the cost-effective extraction of lipids derived from microalgae, which have excellent prospects as alternative biofuels of the future. These lipids principally comprise TAGs, which require the use of structural disruption agents for their efficient extraction.[6] Therefore, there is a huge need to develop strategies to break down and dissolve TAG structures in aqueous solution at or around room temperature.

One suggested approach to cause such disruption has been to use a combination of glucose-derived non-ionic surfactants in combination with small amounts of lipophilic amphiphile.[7,8] Recently, Cui *et al.* reported an alternative approach of using detonation nanodiamonds (NDs) to aid in the removal of crystallised tristearin (TS), a model TAG, at lower temperatures by improving the detergency of the surfactants.[5] NDs produced by the detonation method are hydrophobic, and can adsorb lipid and/or surfactant molecules.[9–11] In their recent study Cui *et al.* investigated the ability of NDs to enhance TS removal, both alone and also in combination with of a variety of different types of surfactant.[5] In the absence of any surfactant the NDs did not promote the removal of TS at room temperatures, where instead the authors suggested the NDs adsorbed to the surface of the crystallised-lipid/water interface. However, when used with surfactants, the NDs were able to aid in the removal of crystallised lipid at room temperature. The NDs were found to be most effective in combination with the anionic surfactant sodium dodecylbenzene sulphonate (SDBS) (the chemical structures of both

[a] *Institute for Frontier Materials, Deakin University, Geelong, Australia. Fax: +61 (0)3 5227 1103; Tel: +61 (0)3 5247 9160; E-mail: zhughes@deakin.edu.au; tiffany.walsh@deakin.edu.au*

† Electronic Supplementary Information (ESI) available: Information on the nanodiamond FF parameters; a summary of the different simulation runs; the chemical structure of TS and SDBS; order parameters for the acyl tails of TS molecules in simulations of Set A and B; area of bilayers as a function of time/temperature for heating simulations of Set B; radial distribution functions of NDs with different species; snapshots of Set D simulations; density profiles of Set D simulations; area of bilayers as a function of time/temperature for heating simulations of Set D; density profiles of Set F and G simulations; snapshots of Set F and G simulations; area of bilayer as a function of time/temperature for the heating simulations of set G. See DOI: 10.1039/b000000x/

TS and SDBS are shown in Fig S1†), where the presence of NDs was able to significantly enhance the removal of TS at both 15 and 25°C. NDs were also found to be effective at enhancing lipid removal in conjunction with use of the non-ionic surfactant β-D-glucopyranoside (G_1C_{10}) at 25°C (but not at 15°C). Minor improvements to the detergency of other surfactants were also reported.

Cui *et al.*[5] hypothesised that the NDs were able to increase the solubilisation of the TS molecules by facilitating roughening of the surface of the crystallised-lipid at the lipid-water interface. However, many open questions remain about the precise role of the NDs in this process. Determination of the molecular-level action of the different species at the lipid aqueous interface is non-trivial from an experimental perspective. Molecular dynamics (MD) simulations, with the ability to probe systems at the atomic level, offer insights that are complementary to experimental data.[12–14] In partnership with experimental efforts, MD simulations can therefore assist in elucidating the molecular-level origins underpinning the room-temperature structural disruption of crystallised lipid in these systems.

Molecular simulation methods have been widely utilised to provide information about the interaction occurring between nanoparticles (NPs) and lipid bilayers at the molecular level.[15–33] A variety of different simulation techniques, including dissipative particle dynamics (DPD),[20,24,28,31,32] both coarse-grained[17,19,21,22,27,30] and atomistic[15,16,18,21,33] MD and Monte Carlo (MC) simulations,[25] have been used to investigate the behaviour of lipid-NP systems over a range of time- and length-scales. The effects of NP properties such as hydrophobicity,[17,19,22,25] size,[21,29,31] shape[20,29,31] and surface functionalisation[15,26,31] have been previously explored. However, in the great majority of these previous studies the lipids modelled were phospholipids (PLs). The headgroup of TAGs, such as TS, are less polar than those of PLs, (especially in the case of the zwitterionic headgroup of phosphocholine (PC), one of most well-studied lipids). This difference in head-group character confers properties of TAG systems that are quite different from those of their PL counterparts in a number of ways.

There have been relatively few atomistic molecular simulations reported for TAGs,[34–41] with the greater part of these previous studies detailing investigations of the bulk phase properties.[34–38] To the authors' knowledge there has been only one study that reported the use of MD simulations to investigate the TAG-aqueous interface.[41] In this study, a TS bilayer in contact with liquid water was simulated at a range of temperatures, both in the presence and absence of the anionic surfactant SDBS. In the absence of any surfactant it was found that below $\approx$ 365 K the TS bilayers were stable in a solid phase, with the lipid tails ordered laterally in a hexagonal structure. Between 365.5-366.7 K the TS bilayers melted, and due to the small size of the polar headgroup, the bilayer structure became unstable. Simulations of the TS bilayers in the presence of SDBS revealed that the surfactant molecules were able to spontaneously insert into the TS bilayer from solution. At 300 K a few insertion events were observed but occurred very infrequently, while simulations at 350 K showed an increase in the number of SDBS molecules that embedded into the bilayer. However, even when the bilayer contained relatively large concentrations of SDBS (a 3:1 ratio of TS:SDBS), only minor changes to the structure of the bilayer were seen. Despite this lack of significant structural change upon incorporation of the surfactant molecules into the TS bilayer, the presence of the inserted SDBS molecules did depress the gel-liquid crystalline phase transition temperature of the bilayer to below 365 K.

In the current work MD simulations have been used to investigate the interaction of NDs with the TS-aqueous interface both in the absence and presence of the anionic surfactant SDBS. The effect of the NDs on the gel-liquid crystalline phase transition temperature has also been explored. Our findings provide strong evidence that confirms current experimental hypotheses regarding the action of the NDs on the room-temperature structural disruption of crystallised lipid.

Methods

All simulations were performed using the GROMACS version 4.6.3.[42] Simulations were performed in the isothermal-isobaric ensemble, *NpT*, with the Nosé-Hoover thermostat[43,44] and Parrinello-Rahman barostat[45] used to maintain the temperature and pressure, respectively. For the simulations where a bilayer was present the pressure in the x, y and z directions were independently coupled to the barostat, otherwise an isotropic pressure coupling was employed. For all simulations the Lennard-Jones non-bonded interactions were switched to zero between 9 and 10 Å, and the electrostatic interactions were evaluated using a particle-mesh Ewald summation,[46] with a real space cutoff of 11 Å.

The CHARMM36 FF was used for TS and SDBS molecules[47,48] (with additional parameters for the SDBS taken from He *et al.*).[49] The water model used was that of the modified version of TIP3P compatible with the CHARMM FF.[50,51] Previous work has shown that CHARMM36 FF is suitable for the simulation of the TS-aqueous interfaces[41] (although there was some evidence that the FF may over-stabilise the TS). Development details for the nanodiamond FF are provided in the ESI† section 'Nanodiamond FF parameters'. The NDs were modelled as $C_{84}H_{64}$ octahedra (measuring $\approx$1.1 nm vertex to vertex). The ND surface was fully hydrogenated. The NDs used in the experimental study of Cui *et al.* were found via ζ-potential measurements to be positively-charged. However, these ζ-potential values cannot readily be directly converted to yield a precise value of the surface charge density of these NDs.[5] Because of this, we considered a range of values for the overall charge on the ND surface, allowing the effect of the ND surface charge density to be explored. Previously-reported calculations indicate that the charge on NDs is localised at the vertices.[52] To capture this in our model, half of the added charge was distributed evenly over the hydrogen atoms attached to the six vertex carbon atoms and the remaining half of the charge was distributed evenly over all the non-vertex hydrogen atoms in the ND. The duration of the MD simulations was 100-300 ns (as indicated in Table S1 in the ESI†), with the last 60 ns of simulation trajectory used for analysis.

The initial structures of the TS bilayers were taken from systems that had previously been equilibrated at 300 or 350 K.[41]

Previous work has found that the structure of pure TS bilayers in contact with liquid water, modelled with the CHARMM 36 FF, break down at $\sim 365.5-367$ K. Therefore, our simulations here were performed at both 300 and 350 K. In addition, a number of simulations where the system was heated were performed to determine the gel/liquid-crystalline phase transition temperature. To better characterise the interactions of the different components of the system (TS, ND and surfactant) a range of different systems were considered. Table S1 of the ESI† provides a summary of each set of simulations. For ease of reference, each specific run is referred to using the following nomenclature of the form $X^{nqi}-j$, where X denotes the class of simulations (see below) of which this run is part, n denotes the number of NDs in the system, qi denotes the surface charge on the NDs in the system, and j indicates the sample number of the run for that system type.

All simulations were conducted under aqueous conditions. The first two sets of simulations (Sets A and B) consisted of the TS bilayers in the presence of NDs, but in the absence of surfactant. For these simulations each system comprised a TS bilayer of 72 molecules (36 molecules per leaflet), 4 NDs, ~7300 water molecules, and a sufficient number of Cl^- counter-ions to ensure overall charge neutrality of the simulation cell. The initial positions of the NDs were randomly assigned within the simulation cell. For the simulations of the three component systems, two different classes of simulations were performed, to explore two key stages of the process of surfactant-assisted, ND-mediated bilayer disruption. In Sets C and D, the ND and SDBS molecules were randomly placed into solution in a simulation cell containing a pure TS bilayer (36 TS molecules per leaflet) pre-equilibrated at the appropriate temperature; 300 K for Set C, and 350 K for Set D. The system was then solvated with ~ 13550 water molecules and Na^+ or Cl^- counter ions to balance the charge of the SDBS/NDs. The purpose of these Set C/D simulations is to investigate the ability of NDs to act as a vector for delivery of the surfactant to the TS bilayer. However, our previous studies indicated that the spontaneous insertion of surfactant from the solution phase into the TS bilayers is associated with very long timescales.[41] While advanced sampling strategies might in future be gainfully applied to explore the timescale of this process, the success of such approaches hinges on an appreciation of the likely initial and final states of this complex pathway. To this end, the Set C and D simulations may capture the initial states of this process, but will not be appropriate for investigating the final stages, *i.e.* how the presence of NDs can affect the stability of TS bilayers that already contain bilayer-embedded surfactant. To explore this latter scenario, we have performed a series of simulations, Sets F and G, based on TS bilayers that contained pre-embedded SDBS molecules over a range of concentrations. In Sets F and G the initial bilayer configuration contained either 16 or 24 SDBS molecules in addition to the 72 TS molecules (having previously been equilibrated at 350 K), with no SDBS molecules present in the solution phase initially (*i.e.* all SDBS were pre-inserted into the TS bilayer structure). The NDs were placed randomly in solution and the system was solvated with ~ 7400 water molecules. The simulations of Sets A and C were performed at 300 K while those of Sets B, D, F and G were performed at 350 K. In order to ensure that the observed results were not anomalous multiple independent samples were simulated for some systems (Sets A^{4q2}, B^{4q0}, B^{4q1}, C^{4q4}, D^{4q4}, F^{4q1}, F^{4q2}, G^{4q1}). These independent samples were not simply extra simulations with distinct initial coordinates and velocities but constructed from different initial TS bilayer structures.[41] At least one system within each class had multiple samples simulated. Systems where the bilayer was strongly affected by the ND/SDBS were always simulated using several samples.

To investigate if the presence of the NDs influenced the temperature that marked the onset of structural disorder in the TS bilayers, additional heating simulations were performed on the resultant structures of the B^{4q0}, B^{4q1}, B^{4q2}, D^{4q4}, F^{4q1}, G^{4q0}, and G^{4q2} systems, following the approach outlined in previous studies.[41,53] In brief, during these heating simulations the temperature was increased from 350 to 370 K over a 200 ns timeframe (*i.e.* at a rate of 0.1 K ns^{-1}). We defined the transition temperature as the temperature average taken over the last 10 ps of the trajectory in the gel phase and the first 10 ps of the trajectory in the liquid crystalline phase. Because the nucleation of a phase transition is a stochastic process, we report the outcomes of more than one simulation for most of our systems. Furthermore, these simulations were used to identify trends in the phase transition temperatures, as opposed to determining specific values.

To investigate the modes of interaction between the surfactant molecules and the NDs in greater depth, simulations considering only SDBS and NDs in aqueous solution, without the presence of a TS bilayer, were also performed (Sets S and T). The systems corresponding to Sets S and T comprised 4 NDs and 20 SDBS molecules in ~13250 water molecules, along with an appropriate number of Cl^- counter-ions to ensure overall charge neutrality. The initial positions of both the NDs and SDBS in the simulation cell were randomly assigned.

Following our previous work,[41] the TS bilayers were characterised by their lateral area, A, membrane thickness D_{HH} (measured as the distance between the two peaks of the TS mass density profile), and peak height H_{max} (measured as the average of the density maximum of the two leaflets in the TS density profile). The degree of ordering in the acyl tails of the lipids can be determined from the order parameter, S_z. S_z for atom C_n (see Fig. S1†) is calculated from

$$S_z = \frac{1}{2}(3\cos^2\theta - 1) \quad (1)$$

where θ is the angle between the z-axis (which is perpendicular to the plane of the bilayer surface) and the vector between C_{n-1} and C_{n+1}.

Results and Discussion

Nanodiamonds with TS bilayers in the absence of SDBS

Table 1 summarises the properties of the TS bilayer and the resulting ND/TS configuration, determined from Sets A and B; namely, simulations of NDs (but not SDBS) in the presence of a pure TS bilayer in aqueous conditions. The properties of TS bilayers in the absence of both NDs and SDBS, determined from previous work (averaged over three simulations), are also provided for reference.[41]

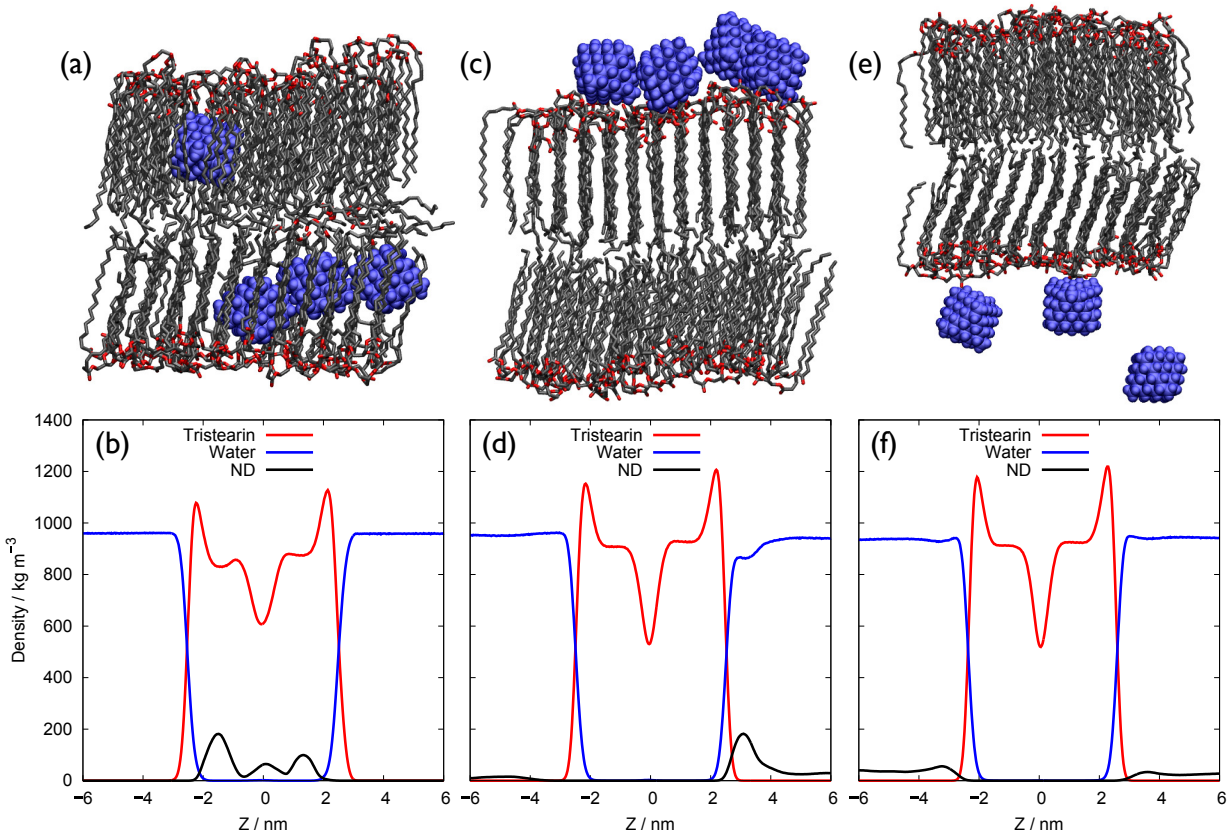

Fig. 1 Snapshots from simulations ((a), (c) and (e)) and density profiles ((b), (d) and (f)) of the TS bilayers in the presence of 4 NDs of different charge: (a) and (b) B^{4q0}-1; (c) and (d) B^{4q1}-1; and (e) and (f) B^{4q2}-1.

Table 1 Summary of simulations of NDs (but not SDBS) in the presence of TS bilayers, along with reference values for aqueous TS bilayers simulated in the absence of NDs and SDBS.[41] The calculated properties of the TS bilayer are the lateral area, A, membrane thickness, D_{HH}, and peak height, H_{max}. 'Remarks' summarises the fate of the NDs as either dispersed in solution, adsorbed to the bilayer surface or embedded in the bilayer.

Run	A / nm^2	D_{HH} / nm	H_{max} / nm	Remarks
A_{Ref}[41]	21.3 ± 0.2	4.54 ± 0.09	1321 ± 32	
B_{Ref}[41]	23.3 ± 0.1	4.35 ± 0.06	1181 ± 16	
A^{4q1}-1	21.4 ± 0.1	4.53	1310	Adsorbed
A^{4q2}-1	21.4 ± 0.1	4.59	1334	Dispersed
A^{4q4}-1	21.5 ± 0.5	4.59	1339	Dispersed
A^{4q4}-2	21.0 ± 0.1	4.61	1336	Dispersed
A^{4q4}-3	21.0 ± 0.4	4.58	1349	Dispersed
B^{4q0}-1	23.7 ± 0.3	4.38	1103	Embedded
B^{4q0}-2	23.9 ± 0.4	4.22	1084	Embedded
B^{4q1}-1	22.9 ± 0.2	4.35	1180	Adsorbed
B^{4q1}-2	23.1 ± 0.3	4.41	1172	Adsorbed
B^{4q2}-1	23.1 ± 0.5	4.33	1198	Dispersed

As our results demonstrate, the hydrophobicity of the uncharged NDs can provide a sufficiently strong driving force to encourage diffusion through the dense TS headgroups and penetrate the **TS** bilayer interior. Figs. 1(a) and (b) show snapshots and density profiles to illustrate this example. Previous simulation studies of the aggregation of uncharged hydrophobic nanoparticles (NPs) within phospholipid (PL) bilayers in the liquid-crystalline phase suggested that the PL bilayer acted as a good solvent for the NP, for NP diameters that were smaller than the PL bilayer thickness.[27,32] In other words, these studies found that NP aggregation within the hydrophobic core of the PL bilayer was limited for for NP diameters that were smaller than the PL bilayer thickness, while this aggregation propensity increased as the NP diameter approached the thickness of the PL bilayer. These previously-reported findings are in contrast to our present work, where we found that NDs with a diameter *smaller* than the TS bilayer thickness (D_{HH}) were able to aggregate within the TS bilayer. This highlights the important differences that exist between liquid-crystalline PL bilayers and the gel phase TS bilayers.

In comparison to the uncharged NDs, we suggest that the NDs that carry a $+1e$ charge are too hydrophilic to enter the hydrophobic core of the bilayer, but instead appear to be attracted to both the TS interface and other NDs, resulting in the adsorption of an aggregate of NDs to the exterior surface of the TS bilayer (Fig. 1(c) and (d)). For systems where the overall charge on the NDs is $+2$ or greater, the NDs did not adsorb to the TS interface, nor did these NDs aggregate. However, the resulting spatial location of these NDs showed a preference for a region just above the surface of the TS bilayer rather than bulk solution (Fig. 1(e) and (f))

In all cases, the overall TS bilayer structure remained stable at 350 K, even in the case the of the penetration of the TS bilayer by the uncharged NDs (although the ordering of the acyl tails was reduced (see Fig. S2†)). Our findings therefore agree with

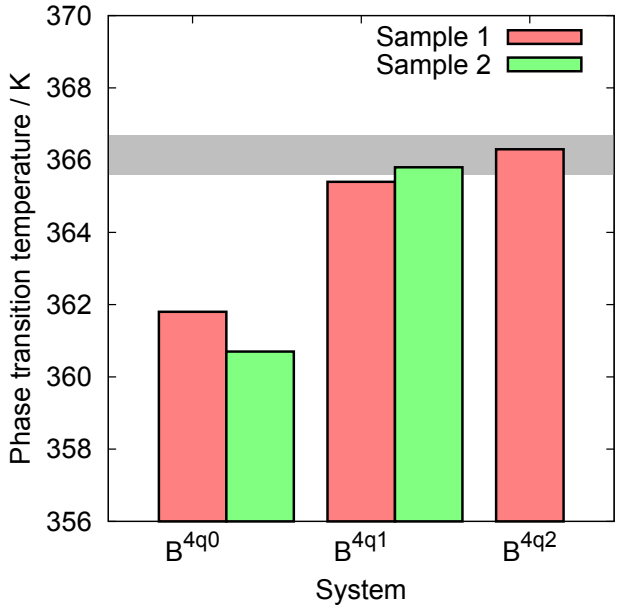

Fig. 2 Phase transition temperatures for simulations in Set B. The shaded grey area indicates the temperature range of the phase transition of TS bilayers in the absence of NDs.

experimental data which found that NDs alone could not facilitate structural disruption of crystallised lipid.[5]

We investigated the stability of the resulting TS bilayer structures as a function of increasing temperature for the Set B systems (NDs and TS, but no surfactant, generated at 350 K). Fig. S3† shows the lateral area of the bilayer as a function of time/temperature, where the lateral area of the bilayer increases linearly with temperature when the bilayer is in the gel phase. Then at the point where the acyl tails of the lipids melt and the phase transition occurs there is a sudden increase in the lateral area of the bilayer. Fig. 2 summarises the phase transition temperatures for the different samples, showing that the systems containing charged NDs supported a phase transition between 365.5–366.7 K, the same temperature range as that of TS bilayers in the absence of any NDs.[41] However, the penetration of the uncharged NDs into the bilayer was seen to reduce the phase transition temperature to ∼361 K. Nonetheless, uncharged nanodiamonds agglomerate in aqueous solution,[5,10,11] meaning that while these NDs may be able to induce a lowering of the phase transition temperature *in theory*, in practice these NDs would not disperse sufficiently to actually produce such phenomena.

Interaction of Nanodiamonds with SDBS in Aqueous Solution

At the solution concentrations used in these simulations, the SDBS molecules aggregated together forming agglomerates. In systems containing both SDBS and NDs in aqueous solution, the NDs were incorporated into these agglomerates. However, the nature of this incorporation, and the resulting morphology of the aggregate, were found to depend upon the charge of the NDs (see below).

Fig. 3 shows representative snapshots of SDBS/ND systems with NDs, as a function of ND surface charge. In the case of charge-neutral NDs, the resulting agglomerate had a core consisting of the NDs, with the surfactant molecules adsorbing to the exterior of the ND agglomerate, via interactions with the SDBS hydrophobic tails. For the NDs carrying a charge of $+2e$ or $+4e$, the structure of the aggregate was reversed, with the SDBS molecules located at the centre of the agglomerate and the NDs adsorbed to the exposed sulphonate headgroups. The ND/SDBS system containing NDs of $+1e$ charge resulted in a structure that was intermediate between these two extreme scenarios.

The effect of ND surface charge on the resulting structure of the aggregate can be seem in more detail in Fig. S4† which shows the radial distribution function between the centre of mass of the NDs with NDs ($g(r)_{\text{ND-ND}}$), water ($g(r)_{\text{ND-W}}$), the sulphonate headgroup of the SDBS molecules ($g(r)_{\text{ND-SH}}$), and the tail of the SDBS molecules ($g(r)_{\text{ND-ST}}$). In the case of the charge-neutral NDs, there is a strong peak in $g(r)_{\text{ND-ND}}$, Fig. S4(a)†, at ~ 1.25 nm, indicating that the NDs are in direct contact with each other in the core of the agglomerate. This peak was substantially diminished for NDs with surface charge of $+1e$, and was absent entirely for NDs with a charge of $+2$ or greater, where the NDs are at the surface of the agglomerate. From $g(r)_{\text{ND-W}}$, Fig. S4(b)†, it is also clear that the hydration of the NDs increased with the surface charge of the NDs. Fig. S4(c) and (d)† show that the interaction of the ND with the surfactant molecule changes as the surface charge on the ND increases, moving from a interaction primarily occurring through the acyl tails of the SDBS for the uncharged NDs, through to an interaction dominated by the sulphonate headgroups for the NDs with $+4e$ surface charge.

Table 2 Summary of simulations of NDs and SDBS in aqueous solution, from Sets C and D. The calculated properties of the TS bilayer are the lateral area, A, membrane thickness, D_{HH}, peak height, H_{max} and the number of SDBS molecules that become embedded in the bilayer, N_{embed}. 'Remarks' summarises the fate of the SDBS/NDs, as either adsorbed to the bilayer surface or embedded in the bilayer.

Run	A / nm^2	D_{HH} / nm	H_{max} / nm	N_{embed}	Remarks
C^{4q2}-1	21.4 ± 0.1	4.54	1314	0	Adsorbed
C^{8q2}-1	21.4 ± 0.1	4.46	1295	1	Adsorbed
C^{4q4}-1	21.4 ± 0.1	4.55	1305	3	Adsorbed
C^{4q4}-2	21.2 ± 0.2	4.67	1311	2	Adsorbed
C^{4q4}-3	21.4 ± 0.2	4.53	1330	1	Adsorbed
C^{8q4}-1	21.4 ± 0.1	4.55	1320	3	Solution
D^{4q0}-1	23.8 ± 0.3	4.43	1077	18	Embedded
D^{4q1}-1	23.4 ± 0.3	4.29	1150	6	Adsorbed
D^{4q2}-1	23.2 ± 0.3	4.33	1170	4	Adsorbed
D^{4q4}-1	23.8 ± 0.6	4.53	1071	20	SDBS Embedded
D^{4q4}-2	23.1 ± 0.3	4.47	1179	6	Adsorbed
D^{4q4}-3	23.2 ± 0.3	4.34	1186	3	Adsorbed
D^{8q4}-1	23.1 ± 0.3	4.49	1205	3	Adsorbed (weak)

Tristearin Bilayers in the Presence of NDs and SDBS

Table 2 summarises the results for the simulations from Sets C and D (consisting of a TS bilayer in the presence of NDs and SDBS molecules, where the SDBS were initially present in the solution phase). As explained in the Methods, the Set C/D simulations have been employed to investigate how the NDs may facilitate the delivery of surfactant to the crystallised lipid surface. Representative snapshots of a number of the systems resulting from the

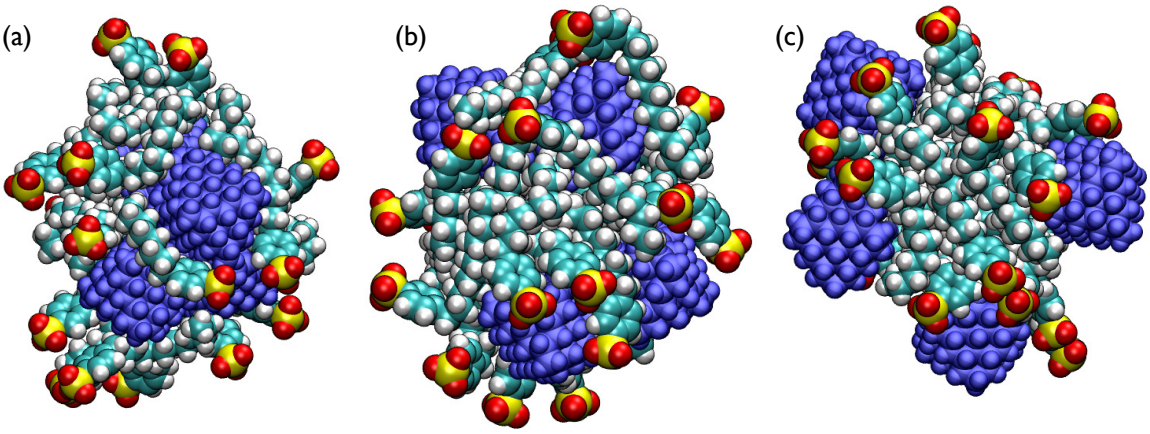

Fig. 3 Snapshots of aggregates formed by NDs in the presence of SDBS: (a) T^{4q0}-1, (b) T^{4q1}-1 and (c) T^{4q2}-1.

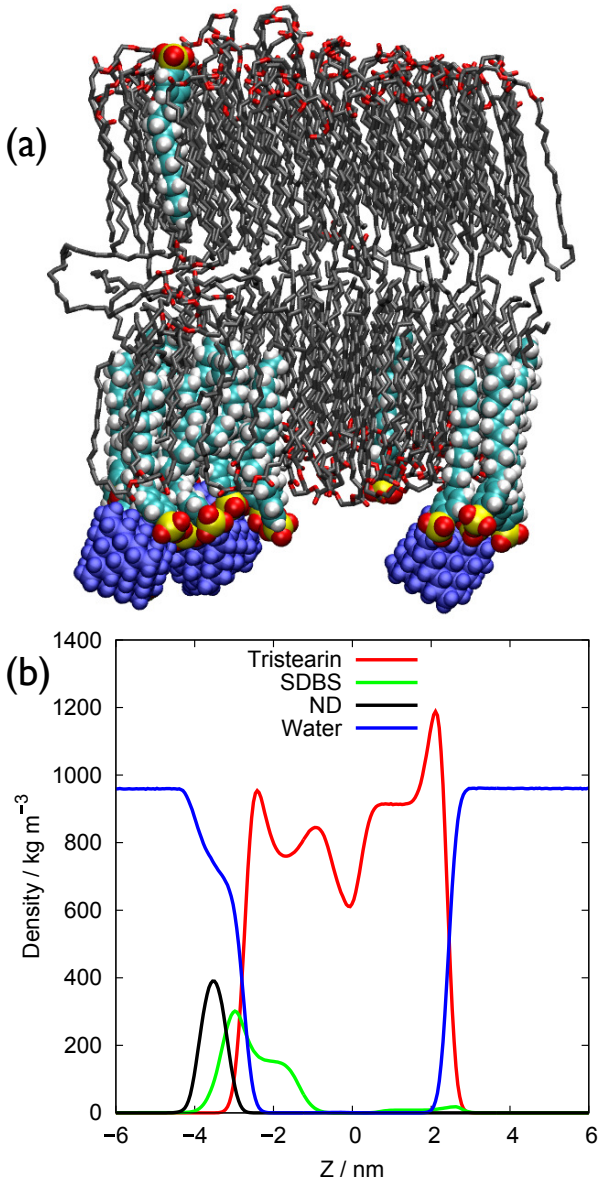

Fig. 4 (a) A representative snapshot and (b) the density profile of the simulation run D^{4q4}-1.

Set D simulations are shown in Fig. 4(a) and Fig. S5†, with the corresponding density profiles of the different systems provided in Fig. 4(b) and Fig. S6†.

In most instances, the SDBS molecules and NDs formed aggregates in solution, which diffused and adsorbed to the surface of the TS bilayer, with a few SDBS molecules actually becoming embedded within the bilayer structure. In simulation C^{8q4}-1 a ND/SDBS agglomerate was formed but did not adsorb to the surface of the bilayer, while in D^{8q4}-1 there was some ND/SDBS adsorption but to a lesser degree than for other class D systems (Fig. S6†). Thus, a high concentration of highly charged NDs (8 NDs with $+4e$ charge) may impede the surface adsorption of ND/SDBS to some extent. Simulations of TS in the presence of SDBS molecules alone (under equivalent conditions) resulted in a few SDBS molecules embedding within the bilayer.[41] However, density profiles show a significantly greater degree of agglomerate surface adsorption for simulations where NDs are present compared with those where they are not.[41] This suggests that NDs could act as an effective vector for the trafficking of surfactant molecules into the TS bilayer.

In the majority of cases, the structure of the TS bilayer was largely unaffected, with only two runs, D^{4q0}-1 and D^{4q4}-1, generating significant structural disruption of the bilayer , see Fig. 4 and Fig. S6†. In the case of D^{4q0}-1 the charge-neutral NDs diffused into the bilayer drawing a significant number of SDBS molecules with them (see Fig. S5(a)†). In the case of D^{4q4}-1 the ND/SDBS agglomerate first adsorbed to the surface of the bilayer before the SDBS molecules in the agglomerate became embedded in the bilayer, with the NDs adsorbed to the surfactant headgroups (see Fig. 4). To determine if the ingress of the NDs and SDBS molecules into the TS bilayer could modify the phase transition temperature of the system, we investigated the stability of the resulting TS bilayer structures as a function of increasing temperature for the structures arising from the D^{4q4}-1 and D^{4q4}-2 simulations. The change in lateral area of the system with time/temperature is shown in Fig. S7†. The phase-transition temperature of the D^{4q4}-2 sample was 364.8 K, just below the range of transition temperatures reported for TS bilayers in the presence of water alone (365.5-367 K[41]), or in the presence of charged NDs

Table 3 Summary of simulations of NDs in the presence of pre-equilibrated TS/SDBS bilayers, Sets F and G, where the SDBS molecules were pre-inserted into the TS bilayer structure. Reference values for the pre-inserted aqueous TS bilayer/SDBS systems simulated in the absence of NDs are also provided.[41] The calculated properties of the TS bilayer are the lateral area, A, membrane thickness, D_{HH}, and peak height, H_{max}. 'Remarks' summarises the fate of the NDs as either adsorbed to the bilayer surface, embedded in the bilayer, or disrupting the bilayer.

Run	A / nm^2	D_{HH} / nm	H_{max} / nm	Remarks
F_{Ref}[41]	25.2 ± 0.3	4.22 ± 0.04	1062 ± 24	Stable
G_{Ref}[41]	25.8 ± 0.1	4.11 ± 0.02	1010 ± 5	Stable
F^{4q1}-1	24.8 ± 0.3	4.31	1096	Adsorbed
F^{4q1}-2	25.4 ± 0.4	4.25	1039	Adsorbed/Embedded
F^{4q2}-1	24.8 ± 0.3	4.30	1091	Adsorbed
F^{4q2}-2	25.4 ± 0.3	4.25	1052	Adsorbed
F^{4q4}-1	25.2 ± 0.3	4.18	1071	Adsorbed
G^{4q0}-1	26.8 ± 0.4	4.24	972	Embedded
G^{4q1}-1	25.6 ± 0.3	-	-	Disrupted
G^{4q1}-2	25.8 ± 0.3	-	-	Disrupted
G^{4q2}-1	25.6 ± 0.3	4.16	1050	Adsorbed
G^{4q4}-1	26.3 ± 0.3	4.12	1034	Adsorbed

alone (Sets B^{4q1} and B^{4q2}, 365.4-366.3 K). The change in the lateral area of the bilayer as a function of temperature (Fig. S7(a)†) was equivalent to those of Sets B^{4q1} and B^{4q2} with both leaflets of the bilayer melting simultaneously. In contrast, at 360.3 K the phase transition temperature for D^{4q4}-1 was significantly lower than that of the D^{4q4}-2 and Sets B^{4q1} and B^{4q2} systems. In this instance the combination of the NDs and SDBS molecules caused the lower leaflet of the bilayer, where the majority of the SDBS were embedded, to undergo a phase-transition before the upper leaflet melted (see Fig. S7(b)†). This result supports the observed experimental data[5] that a combination of SDBS and NDs are able to enhance the structural disruption of crystallised lipid.

In summary, the results of the simulations in Sets C and D suggest that NDs are able to traffic SDBS molecules to the TS bilayer interface, where the surfactant molecules are then able to embed into the bilayer structure. In addition, in some instances the NDs were able to promote the insertion of SDBS molecules, resulting in a reduction in the phase transition temperature of the system. However, the stochastic nature of, and long timescales associated with, the insertion of SDBS molecules into the bilayer makes it challenging at this juncture to determine the precise mechanism(s) by which the NDs are able to disorder the TS bilayer at this lower temperature. As first steps to investigate such phenomena further, we modelled TS bilayers containing 16 or 24 pre-embedded SDBS molecules, summarised in simulation Sets F and G respectively. Previous work showed that TS bilayers containing these ratios of SDBS molecules were stable at 350 K,[41] with the presence of the embedded SDBS exerting little effect on the structure of the TS bilayer.

The results of the Set F and G simulations are summarised in Table 3. Density profiles, snapshots of representative structures and the order parameter for the acyl tails of the TS bilayer (averaged over all three chains) are shown in Figs. S8, S9 and S10 of the ESI†, respectively. As identified from our other simulations, the uncharged NDs diffused into the hydrophobic centre of the

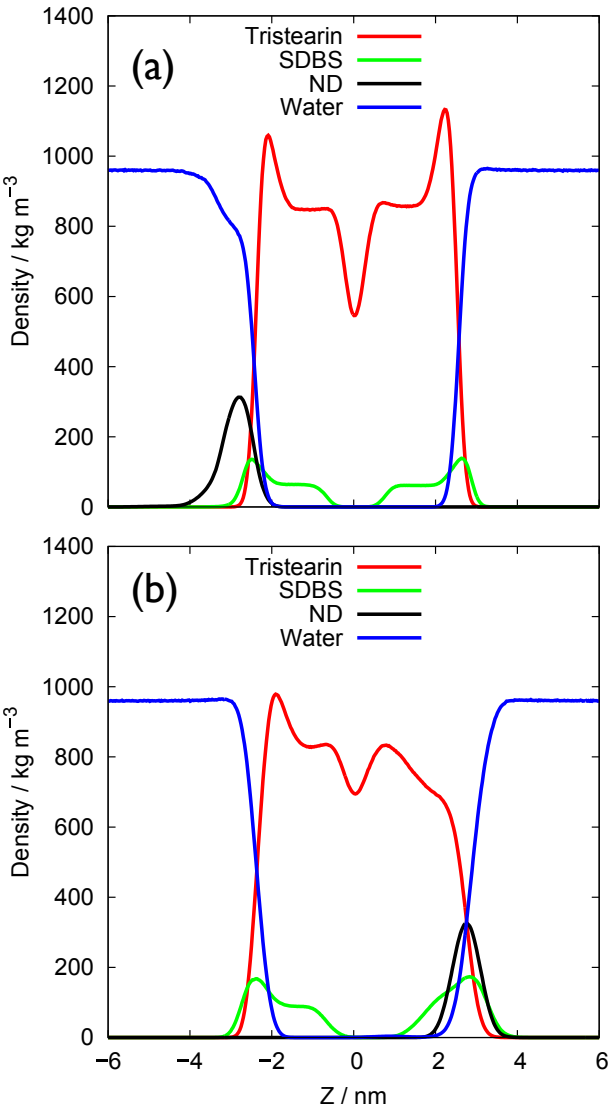

Fig. 5 Density profile of the TS bilayers generated from simulations (a) F^{4q1}-1, and (b) G^{4q1}-1.

TS bilayer structure, (see Fig. S8 and S9[†]). While the presence of the uncharged NDs within the centre of the bilayer did reduce the ordering of acyl tails slightly (Fig. S10[†]), the hexagonal lateral packing of the TS chains remained largely intact. However, the presence of pre-embedded SDBS molecules appeared to encourage the adsorption of charged NDs at the aqueous TS/SDBS-bilayer interface, even for NDs carrying a $+4e$ charge. However, the most interesting behaviour was observed in the case of NDs carrying an overall charge of $+1e$. For those bilayers with a TS:SDBS ratio of 4.5:1 (Set F) the NDs not only adsorbed at the bilayer interface but were also able to partially embed into the upper leaflet of the bilayer, Fig. 5(a). For the Set G bilayers (those with a TS:SDBS ratio of 3:1) this partial embedding outcome was even more pronounced, with marked disruption of structure of the bilayer leaflet in the vicinity where the NDs were adsorbed, see Fig. 5(b). In fact, our simulations indicate that the combination of NDs and SDBS can induce a spontaneous phase-transition with the lipid tails of the leaflet where the NDs adsorbed. In both samples of Set G^{4q1} the acyl tails of the lipids were melted in leaflet to which the NDs had adsorbed at 350 K, as shown in Fig. 6(a). In the absence of NDs, those bilayers with a 3:1 ratio of TS:SDBS did not undergo a phase transition until 358-364 K.[41] The phase transition temperatures of the G^{4q0} and G^{4q2} systems were found to lie within the 358–364 K control range, Fig. 6(b) and S11[†]. This indicates that the surface charge density on the NDs is key to lowering inducing disruption of the TS bilayer at lower temperatures. While still in the gel phase at 350 K, our heating simulations of the F^{4q1} systems showed that for bilayers with a TS:SDBS ratio of 4.5:1 in the presence of NDs the phase transition temperatures were 357.5 and 358.9 K, towards the lower end of the temperature range of the class G bilayers, Fig. 6(b) and S11[†].

Our findings suggest that NDs with $+1e$ charge are effective at promoting the phase change of the TS/SDBS bilayers. We propose that the reasons for this can be attributed to the ability of the $+1e$ charged NDs to interact favourably with both the head and tail groups of the surfactant molecules. In contrast, the uncharged NDs appear to be too hydrophobic to interact with the surfactant headgroups, while the driving force for these NDs to penetrate into the hydrophobic core of the bilayer appeared very strong. The NDs carrying a surface charge of $+4e$ interacted with SDBS principally via the sulphonate headgroups and adsorbed to the surface of the TS bilayer, but did not interact substantially with the hydrophobic acyl tails (see Fig. S4[†]). NDs that carried a $+1e$ or $+2e$ charge were able to interact favourably with both the heads and the tails of SDBS, as indicated by the strong peak in both $g(r)_{\text{ND-SH}}$ and $g(r)_{\text{ND-ST}}$, Fig. S4(c) and (d)[†], for these NDs. However, while the NDs that carried a $+2e$ charge were not too hydrophilic to interact with the acyl tails of the surfactant molecules, they appeared to be too hydrophilic to spontaneously embed into the TS bilayer structure. In contrast the NDs with $+1e$ charge were observed to embed (either fully, Set G, or partially, Set F) into the TS bilayer, provided that SDBS molecules were available to wrap around the surface of these NDs. The ingress of these SDBS-wrapped NDs appeared to disrupt the well-ordered hexagonal lateral packing of the TS bilayer[41] and concomitantly

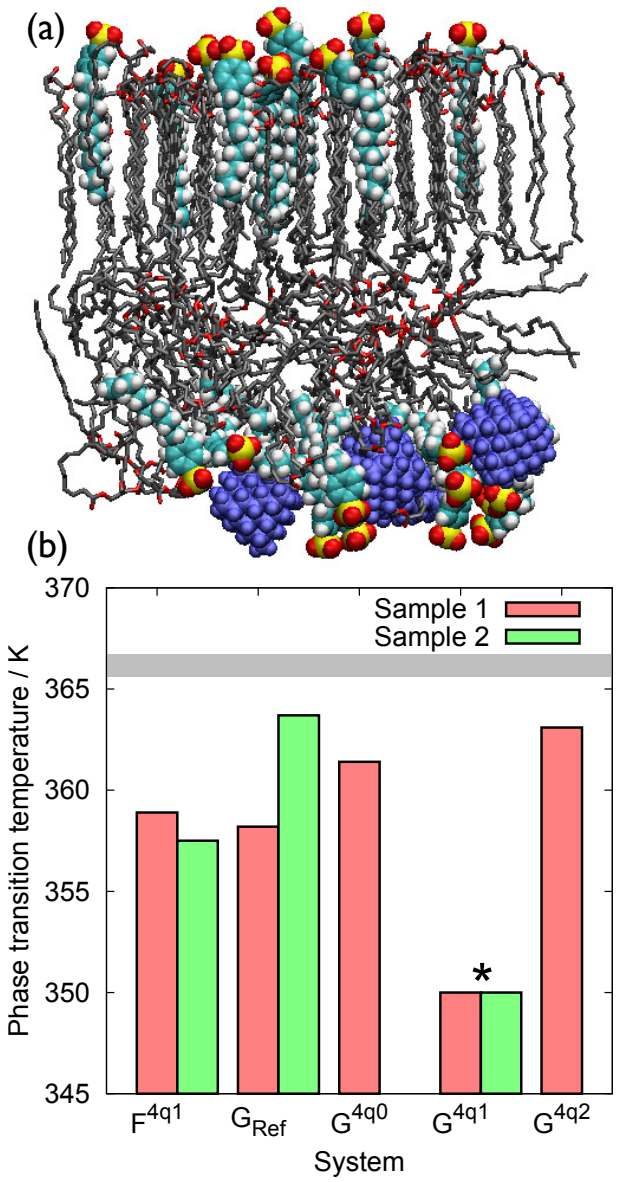

Fig. 6 Set F and G simulations: (a) Snapshot of G^{4q1}-1 showing a lower leaflet phase transition. (b) Phase transition temperatures for Sets F and G. G_{Ref} refers to the 3:1 TS:SDBS bilayers in the absence of any NDs.[41] The shaded grey area in indicates the temperature range of the phase transition of TS bilayers in the absence of NDs and/or SDBS. * indicates a spontaneous phase transition at 350 K.

reduced the stability of the system.

While the complete solubilisation of the TS bilayer was not observed in any of our simulations, this outcome is not surprising or unreasonable considering the time-scales and length-scales accessible to these simulations. By practical necessity, the diameter of the NDs used in our simulations, ~ 1 nm, is smaller than the NDs used in the experiments of Cui *et al.*, ~ 5 nm, to ensure that a reasonable compromise can be reached between the lengthscales and timescales inherent to this system, and their corresponding computational demands. Even so, the relative lengthscale of the NDs with respect to the lateral area of the bilayers considered here ($\sim 5 \times 5$ nm^2) will be considerably greater than that of experiment. In addition, the ratio of the ND diameter to the bilayer thickness, which has been suggested to affect the propensity of hydrophobic (uncharged) NPs to aggregate in PL bilayers,[27,32] will be smaller in the simulations than in the experiments. Moreover, in contrast to our simulations, in an experimental setting the distribution of the ND diameters and charge densities is unlikely to be monodisperse, and will more likely possess a range of size and surface charge densities, which could affect our results.[54,55] The effects of ND diameter (in relation to the TS bilayer thickness) and sample polydispersity would be challenging to investigate using atomistic simulations at present. However, the development of a CG model, based on the results of our present study, would allow such factors to be investigated in future. Further, only the total amount of charge on the ND has been varied in our simulations, not the *distribution* of charge over the ND surface. Investigation of this, as well as the effect of surface functionalisation of the NDs, are areas for future studies. Finally, one further avenue for future study would be the investigation of whether nanomaterials other than nanodiamonds are also able to disrupt the structure of TAG bilayers. Our results indicate that a key property required of such nanomaterials would be a balanced degree of hydrophobicity and surface charge, suggesting that other nanomaterials might be effective in the removal of crystallised lipid.

Despite the limitations outlined above, there is general agreement between our simulations and key experimental findings. First, in our simulations for Set A and B (*i.e.* TS bilayers in the presence of NDs alone in solution), the NDs with a surface charge less than or equal to $+1e$ did adsorb to the TS bilayer surface. This agrees with the observation of Cui *et al.* that in the absence of SDBS, NDs with a low zeta potential adsorbed to the crystallised lipid substrate. Second, our finding that the hydrophobicity of the NDs is a key parameter that can control the nature of ND interaction with both the surfactant and crystallised lipid surface agrees with experimental observations.[5] In these experiments, it was found that the rate of removal of TS from the crystallised lipid substrate was inversely proportional to the strength of the electrostatic interaction between the SDBS and the NDs. This modulation of the interaction between NP and bilayer through control of the hydrophobicity has also been demonstrated experimentally for other systems.[13,14] Third, Cui *et al.* found stronger mass adsorption to the lipid surface in the presence of surfactant and NDs than for surfactant alone. This also agrees with our simulation data that found the SDBS/ND agglomerates to be more likely to adsorb to the lipid surface than agglomerates consisting solely of SDBS.

Conclusions

In agreement with experimental data, our molecular dynamics simulations predicted that use of NDs alone was not sufficient to drive the structural disruption of crystallised lipid (tristearin, TS), but that the use of nanodiamonds in the presence of surfactant could lower the temperature at which disruption of the tristearin bilayer could be observed. Our results indicate that the ND surface charge influenced the mode of interaction between the NDs and both the lipid and surfactant molecules. Specifically, this charge controlled the balance between electrostatic attraction between the surfactant head-group and the charged ND surface, and the hydrophobic interaction between the NDs, the acyl tails of the surfactant, and the TS molecules.

This balance of ND hydrophobicity and hydrophilicity controlled the agglomerate morphology of the NDs and surfactant molecules in solution. An optimal surface charge on the NDs of $+1e$ resulted in adsorption of these agglomerates to the TS bilayer surface, where the surfactant could consequently embed into the bilayer. Additional simulations of NDs in the presence of TS bilayers containing pre-embedded SDBS molecules revealed either adsorption or bilayer penetration, with the most substantial effect seen for NDs with a $+1e$ charge, which roughened the bilayer surface. This structural disruption of the lipid bilayer was accompanied by a depression in the gel-liquid crystalline phase transition temperature for bilayers with a TS:SDBS ratio above a critical threshold. Our simulations provide detailed molecular insights into the mechanisms by which NDs can enhance tristearin removal in the presence of surfactant. These findings will assist the pursuit of knowledge-based refinement of ND/surfactant formulations for realising low-temperature structural disruption and removal of crystallised lipid.

Acknowledgments

This research was undertaken with the resources of the National Computational Infrastructure (NCI), which is supported by the Australian Government. TRW thanks **veski** for an Innovation Fellowship. ZEH thanks the Victorian Life Sciences Computational Initiative (VLSCI) for a travel grant.

References

1 C. Pakula and R. Stamminger, *Energy Efficiency*, 2010, **3**, 365–382.

2 C. A. Miller and K. H. Raney, *Colloid Surf. A* , 1993, **74**, 169–215.

3 A. W. Sonesson, T. H. Callisen, U. M. Elofsson and H. Brismar, *J. Surfactant Deterg.*, 2007, **10**, 211–218.

4 K. Thirunavukarasu, N. G. Edwinoliver, S. Durai Anbarasan, M. K. Gowthaman, H. Iefuji and N. R. Kamini, *Process Biochem.*, 2008, **43**, 701–706.

5 X. Cui, X. Liu, A. S. Tatton, S. P. Brown, H. Ye and A. Marsh, *ACS Appl. Mater. Interfaces*, 2012, **4**, 3225–3232.

6 Y. S. Lai, F. De Francesco, A. Aguinaga, P. Parameswaran and B. E. Rittmann, *Green Chem.*, 2016, **18**, 1319–1326.

7 C. Tongcumpou, E. J. Acosta, L. B. Quencer, A. F. Joseph, J. F. Scamehorn, D. A. Sabatini, S. Chavadej and N. Yanumet, *J Surfactant Deterg.*, 2003, **6**, 205–214.

8 P. Tanthakit, A. Nakrachata-Amorn, J. F. Scamehorn, D. A. Sabatini, C. Tongcumpou and S. Chavadej, *J. Surfactant Deterg.*, 2009, **12**, 173–183.

9 A. P. Puzyr, A. V. Baron, K. V. Purtov and E. V. Bortnikov, *Diam. Relat. Mater.*, 2007, **16**, 2124–2128.

10 A. Krueger, *Adv. Mater.*, 2008, **20**, 2445–2449.

11 A. Krueger, *J. Mater. Chem.*, 2011, **21**, 12571.

12 P. R. Leroueil, S. A. Berry, K. Duthie, G. Han, V. M. Rotello, D. Q. McNerny, J. R. Baker, B. G. Orr and M. M. Banaszak Holl, *Nano Lett.*, 2008, **8**, 420–424.

13 H.-Y. Lee, S. H. R. Shin, L. L. Abezgauz, S. A. Lewis, A. M. Chirsan, D. D. Danino and K. J. M. Bishop, *J. Am. Chem. Soc.*, 2013, **135**, 5950–5953.

14 B. B. Manshian, D. F. Moyano, N. Corthout, S. Munck, U. Himmelreich, V. M. Rotello and S. J. Soenen, *Biomaterials*, 2014, **35**, 9941–9950.

15 R. Qiao, A. P. Roberts, A. S. Mount, S. J. Klaine and P. C. Ke, *Nano Lett.*, 2007, **7**, 614–619.

16 S. Choe, R. Chang, J. Jeon and A. Violi, *Biophys. J.*, 2008, **95**, 4102–4114.

17 Y. Li, X. Chen and N. Gu, *J. Phys. Chem. B*, 2008, **112**, 16647–16653.

18 S. L. Fiedler and A. Violi, *Biophys. J*, 2010, **99**, 144–152.

19 Y. Li and N. Gu, *J. Phys. Chem. B*, 2010, **114**, 2749–2754.

20 K. Yang and Y.-Q. Ma, *Nat. Nanotech.*, 2010, **5**, 579–583.

21 A. Jusufi, R. H. DeVane, W. Shinoda and M. L. Klein, *Soft Matter*, 2011, **7**, 1139–1146.

22 J. P. Prates Ramalho, P. Gkeka and L. Sarkisov, *Langmuir*, 2011, **27**, 3723–3730.

23 R. C. Van Lehn and A. Alexander-Katz, *Soft Matter*, 2011, **7**, 11392.

24 Y. Li, X. Li, Z. Li and H. Gao, *Nanoscale*, 2012, **4**, 3768.

25 S. Pogodin, M. Werner, J.-U. Sommer and V. A. Baulin, *ACS Nano*, 2012, **6**, 10555–10561.

26 R. C. Van Lehn, P. U. Atukorale, R. P. Carney, Y.-S. Yang, F. Stellacci, D. J. Irvine and A. Alexander-Katz, *Nano Lett.*, 2013, **13**, 4060–4067.

27 J. Barnoud, G. Rossi and L. Monticelli, *Phys. Rev. Lett.*, 2014, **112**, 068102.

28 D. L. Cheung, *J. Chem. Phys.*, 2014, **141**, 194908.

29 H.-m. Ding and Y.-Q. Ma, *Small*, 2014, **11**, 1055–1071.

30 G.-X. Guo, L. Zhang and Y. Zhang, *Front. Phys.*, 2015, **10**, 177–186.

31 Z. Ge, Q. Li and Y. Wang, *J. Chem. Theory Comput.*, 2014, **10**, 2751–2758.

32 F. Tian, X. Zhang and W. Dong, *Phys. Rev. E*, 2014, **90**, 052701.

33 M. Thomas, M. Enciso and T. A. Hilder, *J. Phys. Chem. B*, 2015, **119**, 4929–4936.

34 A. K. Sum, M. J. Biddy, J. J. de Pablo and M. J. Tupy, *J. Phys. Chem. B*, 2003, **107**, 14443–14451.

35 A. Hall, J. Repakova and I. Vattulainen, *J Phys. Chem. B*, 2008, **112**, 13772–13782.

36 W.-D. Hsu and A. Violi, *J. Phys. Chem. B*, 2009, **113**, 887–893.

37 D. A. Pink, C. B. Hanna, C. Sandt, A. J. MacDonald, R. MacEachern, R. Corkery and D. Rousseau, *J. Chem. Phys.*, 2010, **132**, 054502.

38 A. Brasiello, S. Crescitelli and G. Milano, *Farad. Discuss.*, 2012, **158**, 479–492.

39 M. Greiner, A. M. Reilly and H. Briesen, *J. Agri. Food Chem.*, 2012, **60**, 5243–5249.

40 M. Greiner, B. Sonnleitner, M. Mailänder and H. Briesen, *Food & Function*, 2014, **5**, 235–242.

41 Z. E. Hughes and T. R. Walsh, *RSC Advances*, 2015, **5**, 49933–49943.

42 B. Hess, C. Kutzner, D. Van Der Spoel and E. Lindahl, *J. Chem. Theory Comput.*, 2008, **4**, 435–447.

43 S. Nosé, *J. Chem. Phys.*, 1984, **81**, 511–519.

44 W. Hoover, *Phys. Rev. A*, 1985, **31**, 1695–1697.

45 M. Parrinello and A. Rahman, *J. Appl. Phys.*, 1981, **52**, 7182–7190.

46 T. Darden, D. York and L. Pedersen, *J. Chem. Phys.*, 1993, **98**, 10089–10092.

47 J. B. Klauda, R. M. Venable, J. A. Freites, J. W. O'Connor, D. J. Tobias, C. Mondragon-Ramirez, I. Vorobyov, A. D. MacKerell, Jr. and R. W. Pastor, *J. Phys. Chem. B*, 2010, **114**, 7830–7843.

48 R. W. Pastor and A. D. MacKerell, Jr, *J. Phys. Chem. Lett.*, 2011, **2**, 1526–1532.

49 X. He, O. Guvench, A. D. MacKerell, Jr. and M. L. Klein, *J. Phys. Chem. B*, 2010, **114**, 9787–9794.

50 W. L. Jorgensen, J. Chandrasekhar, J. D. Madura, R. W. Impey and M. L. Klein, *J. Chem. Phys.*, 1983, **79**, 926.

51 E. Neria, S. Fischer and M. Karplus, *J. Chem. Phys.*, 1996, **105**, 1902–1921.

52 A. S. Barnard and M. Sternberg, *J. Mater. Chem.*, 2007, **17**, 4811–4819.

53 S. Leekumjorn and A. K. Sum, *Biochim. Biophys. Acta - Biomembr.*, 2007, **1768**, 354–365.

54 A. S. Barnard, *ACS Nano*, 2014, **8**, 6520–6525.

55 M. Fernandez and A. S. Barnard, *ACS Nano*, 2015, **9**, 11980–11992.